Nonequilibrium molecular dynamics simulation of shear-induced alignment of amphiphilic model systems

Hongxia Guo, Kurt Kremer, and Thomas Soddemann
Max-Planck-Institut für Polymerforschung, Ackermannweg 10, 55128 Mainz, Germany
(Received 14 March 2002; published 18 December 2002)

We study the shear-induced alignment transition from transverse to the shear plane to parallel and perpendicular in a lamellar or smectics system. A recently proposed simple continuum model for amphiphiles is studied by large-scale nonequilibrium molecular dynamics simulation. We find a shear-rate dependence of the alignment transition under shear flow, parallel at low and perpendicular alignment at high shear rates. To identify the alignment and degree of order of these shear-induced orientations by scattering, a 3D analysis of the scattering data is needed.

DOI: 10.1103/PhysRevE.66.061503 PACS number(s): 83.10.Rs, 82.70.Uv, 83.10.Tv, 83.50.Ax

I. INTRODUCTION

The properties of amphiphilic systems such as diblock copolymers and surfactants and of liquid crystals display a wealth of physical phenomena of both fundamental physical, biological, and technological importance. There has been substantial work on exploring their rich equilibrium phase behavior in the past and a very well understanding has been achieved by today [1–5]. In addition, there is much current interest in nonequilibrium behavior of these complex fluids i.e., under shear flow [6–12] and new phases have been discovered. For example, Diat and Roux [8] discovered multilamellar vesicles forming under high shear in lyotropic systems. These so-called onion phases are still subject to extensive experimental research and very difficult to access by theoretical means. On the other hand there are diblock copolymers, whose lamellar equilibrium phase is subject to reorientation when those systems are sheared. Similarly smectic liquid crystals display the very same basic behavior. Hence, it is desirable to have the ability to predict the orientation of those lamellae. Under shear, molecules realign to the favorable (low frictional) structures. Both *ex situ* measurements such as transmission electron microscopy, small angle x-ray scattering (SAXS), and small angle neutron scattering of the final state as well as scattering and flow birefringence experiments directly applied under shear have been performed. They provide a wealth of information on the possible shear-induced orientation transformations. On the theory side, Fredrickson [11] and Drolet *et al.* [12] studied the stability of the lamellar phase of diblock copolymers under shear flow.

Three obvious orientations with respect to the shearing plates can be defined: parallel with a layer normal in the velocity gradient direction, transverse with a layer normal along the flow direction, and perpendicular with a layer normal in the vorticity direction. In the case of diblock copolymers and smectic liquid crystals, the lamellae of a sheared sample tend to order, reorder, or reorient, depending on shear rate or frequency, into one of the above orientations. The transverse orientation certainly is most unstable upon the application of shear. However, the dynamics from transverse to more favorable orientations in a lyotropic liquid crystal system was not monitored directly until recently by Golan *et al.* [13], who successfully followed the gradual transition from transverse to perpendicular orientation in a lamellar phase by recording the SAXS spectra in the two-dimensional velocity-voriticity plane. They found that the maximum of final perpendicular alignment peak in the SAXS spectra was seemingly smaller than that of initial transverse alignment peak in the spectra of their Fig. 3(c), indicating a somewhat reduced degree of order.

Experiments on other lamellar systems have shown the existence of parallel or perpendicular orientations as a function of shear rate [7,9]. Therefore, as illustrated in Fig. 1, besides perpendicular orientation the transverse alignment can also transform into the parallel alignment under certain shear conditions. To fully characterize these shear-induced alignments, 3D scattering spectra are needed, which are experimentally not available. In addition, the experiments cannot provide any spacial resolution, which would be needed in order to identify the underlying mechanism. Thus the details of the transverse domain tilting to the perpendicular orientation and the inter-relation between the flow, structures, and rheological properties are still unclear.

Recently, some of us published a simple model for the effective large-scale simulation of amphiphilic systems [14]. In the present work, we study the behavior of transverse-oriented lamellar systems under shear by molecular dynamics simulations applying the same model. We find that depending on the shear rate one is able to identify a transition from transverse to perpendicular or transverse to parallel. The paper is organized as follows: In the following section the simulation model and methods are briefly reviewed. This is followed by a presentation of the simulation results and discussion of the findings. Thereafter, we calculate the scattering function and discuss them in the context of the experimental results. In the concluding remarks we summarize the main findings of this paper.

II. MODEL AND METHODS

There are several simulation studies on lamellar systems employing models for mesogenes forming smectic liquid crystals [15], surfactants or lipids [16] as well as block copolymers in the lamellar phase [17,18] in the recent literature. However, the chosen models require typically computer

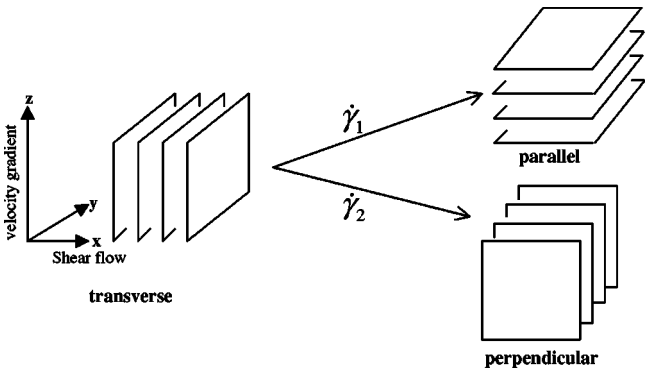

FIG. 1. The sketch of the coordinate system and possible transition from initial transverse alignment to the parallel and the perpendicular orientation.

rescourses, which only allow to study fairly small systems, taking the total number of amphiphilic molecules or mesogenes considered. In the following we briefly review the simulation model for amphiphilic dimers introduced by some of us earlier [14]. The basic ingredients of this model are particles that interact through spherically symmetric potentials.

Like most molecular dynamics (MD) simulation all particles exhibit a hard core that provides an effective excluded volume. A convenient choice for this is a Lennard-Jones (LJ) potential that is truncated at the minimum, and shifted,

$$U_{\mathrm{LJ}}=\begin{cases} 4\epsilon\left[\left(\dfrac{\sigma}{r}\right)^{12}-\left(\dfrac{\sigma}{r}\right)^{6}+\dfrac{1}{4}\right] & r\leqslant 2^{1/6}\sigma \\ 0 & r\geqslant 2^{1/6}\sigma, \end{cases} \tag{1}$$

where ϵ, σ, and r are the energy scale, the length scale, and the distance between particles.

As a minimal model for amphiphilic molecules, we only consider dimers of different species. From polymer simulations [19,20] it is known that it is computationally efficient to link the dimers via anharmonic FENE (''finitely extensible nonlinear elastic'') springs with spring constant k and maximum extension R_0,

$$U_{\mathrm{FENE}}=\begin{cases} -\dfrac{1}{2}kR_0^2\ln\left[1-\left(\dfrac{r}{R_0}\right)^2\right] & r<R_0 \\ \infty & r\geqslant R_0. \end{cases} \tag{2}$$

The parameters for the FENE potential are chosen to be $k=5$ and $R_0=2$.

In order to introduce a bias towards phase separation, like particles have in addition to their hard core interaction an attractive tail in their potential. The like-particle interaction is simulated by adding a cosine wave to a hard core Lennard-Jones, and is given by

$$U_{\mathrm{LJcos}}=\begin{cases} 4\epsilon\left[\left(\dfrac{\sigma}{r}\right)^{12}-\left(\dfrac{\sigma}{r}\right)^{6}+\dfrac{1}{4}\right]-\phi & r\leqslant 2^{1/6}\sigma \\ \dfrac{1}{2}\phi[\cos(\alpha r^2+\beta)-1] & 2^{1/6}\sigma\leqslant r\leqslant 1.5 \\ 0 & r\geqslant 1.5. \end{cases} \tag{3}$$

Here ϕ is the depth of the attractive well, essentially playing the role of an inverse temperature. α and β are determined as the solutions of the linear set of equations

$$2^{1/3}\alpha+\beta=\pi, \tag{4}$$

$$2.25\alpha+\beta=2\pi, \tag{5}$$

i.e., $\alpha=3.173\,072\,867\,8$ and $\beta=-0.856\,228\,645\,44$.

With this set of potentials a dimeric melt (*AB* dimers) is simulated with molecular dynamics method in the *NVT* ensemble. The dimer *A* and *B* beads are connected by the FENE spring. They serve as a coarse grained, miniminal mesoscopic model of diblock copolymers or small surfactants. These systems exhibit a first-order transition from a disordered to a lamellar phase at a potential depth of about $\phi=1.2$ [14]. A nematic phase is not accessible with the choice of such a system as shown by Morse and Milner [21].

In the present study all our systems are taken to be at the same fixed temperature $k_BT=1.0$, while ϕ is slightly varied, in order to run through the order-disorder phase transition. For simplicity, we apply standard Lennard-Jones units for the energy and length scale with $\epsilon=\sigma=1.0$ for all particles. The simulations were carried out at constant volume at a time step of $\delta t=0.01\tau$, where τ is the time scale given by $\tau=(\sigma^2m/\epsilon)^{1/2}$. For the integration of the equations of motion, we employed a standard velocity Verlet algorithm. The overall monomer number density is set to $\rho=0.85$. Periodic boundary conditions are applied in all three dimensions. Obviously, such a model is a very reduced representative of the most studied case of a conformationally symmetric amphiphilic systems such as PEE-PEP (polyethylethylene-polyethylene-alt-propylene, disregarding any entanglement effects), where the components have a small mechanical contrast.

Shear is applied to the simulation systems via an extended version of an algorithm introduced by Müller-Plathe [22]. This algorithm is based on momentum transport within the system to achieve a certain velocity gradient and originated from a nonequilibrium molecular dynamics method for obtaining thermal conductivities and Soret coefficients. The important features of this algorithm concerning our application and modifications have been explained in elsewhere [23,29]. The velocity gradient in our system is given by $\nabla_z v_x$. The shear viscosity η relates the momentum flux $j_z(p_x)$ and this gradient tensor via

$$j_z(p_x)=-\eta\nabla_z v_x. \tag{6}$$

A flux like this can always be described as a transport through a surface perpendicular to its direction within a time interval Δt. In Müller-Plathe's algorithmm the momentum

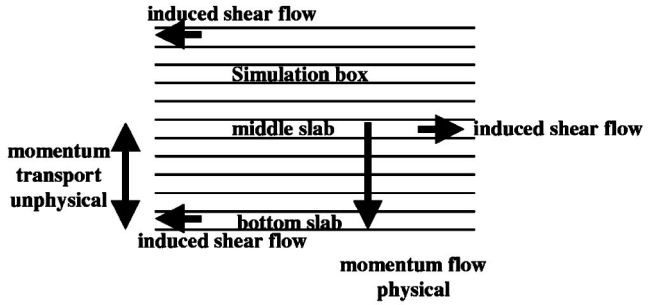

FIG. 2. The sketch of the shear algorithm. For details see text.

flux is imposed in an unphysical way. As illustrated in Fig. 2, the simulation box of size L_x, L_y, and L_z is subdivided into N_{sl} slabs along the velocity gradient direction z with thickness Δd. The middle slab at position $z=L_z/2$ and the bottom slab at position $z=0$ are picked out. Both slabs have a designated preferred direction of flow, e.g., the middle slab towards $+x$, the bottom slab towards $-x$. In the original algorithm one searches the two particles in both slabs, which move fastest against the preferred directions and exchanges their momenta. By doing so, momentum (Δp_x) is transfered across the system. Such exchanges are performed at a fixed rate and the total transferred momentum in Δt is given by $P_x=\Sigma\Delta p_x$. The response of the system to this nonequilibrium excitation is a momentum flux into the opposite direction via a physical mechanism, the friction. In a steady state, transport and flux are equal,

$$j_z(p_x)=\frac{P_x}{2L_xL_y\Delta t}. \tag{7}$$

The momentum flux leads to a continuous velocity gradient in the fluid and the mean velocity of each slab is given by the average over the particles belonging to it. Due to the transport of momenta the flux $j_z(p_x)$ is exactly known. Given a shear rate, the shear viscosity can be derived by

$$\eta=\frac{P_x}{2L_xL_y\Delta t\dot{\gamma}}. \tag{8}$$

As described in our earlier work, we use an extended version and keep a given strain rate constant by repeated interchanges of momenta. For thermostating the nonequilibrium simulation we make use of the DPD thermostat which we have already successfully applied in our earlier simulation. For details of implementation with the DPD thermostat we refer to Ref. [23]. We should mention that our approach is different from that usually employed for anisotropic systems. A thorough review of alternative methods can be found in Ref. [32].

The structural evolution as a function of shear rate and time is monitored by snapshots of particles in the box, pressure tensor, instantaneous viscosities, and by the time-resolved structure factor. The degree of orientational order is measured through the symmetric, traceless Saupe tensor [24]

$$Q_{\alpha\beta}=\frac{3}{2}(\hat{r}_\alpha\hat{r}_\beta-\tfrac{1}{3}\delta_{\alpha\beta}), \tag{9}$$

where α and β are Cartesian indices, δ is the Kronecker symbol, and $\hat{\mathbf{r}}$ denotes a unit vector along the molecular axis. In the unaxial nematic phase, the volume average of $Q_{\alpha\beta}$ has three eigenvalues $(S,-S/2,-S/2)$, where $S>0$ is the order parameter and its eigenvector $\hat{\mathbf{n}}$ is the orientation of director. S is zero in the isotropic state and it approaches unity for the hypothetically perfect monodomain molecular alignment. The nematic director $\hat{\mathbf{n}}$ is a unit vector describing the average direction along which the molecules point. For example, in the present simulation geometry, the perfect transverse lamellar phase has the only nonzero director component of $n_x=1$, the parallel lamellar phase has the only nonzero director component of $n_z=1$, and the perpendicular phase has the only nonzero director component of $n_y=1$. Note that in the lamellar (smectic) phase, especially under shear, $\hat{\mathbf{n}}$ is not necessarily parallel to the layer normal! The pressure tensor is measured via the virial theorem by considering the conservative force $\mathbf{F}$ contribution and the momentum distribution [25]

$$P_{\alpha\beta}=\frac{1}{V}\left\langle\sum_i m_i v_{i,\alpha}v_{i,\beta}\right\rangle+\frac{1}{V}\left\langle\sum_i\sum_{j>i}F_{ij,\alpha}\cdot r_{ij,\beta}\right\rangle, \tag{10}$$

where $\mathbf{v}_i$ is the velocity of monomer i and V is the volume of the simulation box. In the isotropic case the bulk pressure is equal to one third the trace of the pressure tensor. At each state point, systems are equilibrated for at least 4000τ until a steady state is attained. Then the shear is introduced. All data, except those instant response functions to monitor the structural evolution, are calculated after the system again has reached the steady state.

III. SIMULATION RESULTS

When the model was introduced, the general aspects were tested in detail [14]. For the present work we first improve the precision in the location of the isotropic lamellar phase transition point. For this we have performed a series of equilibrium MD simulations on a system size of $N=101\,306$ particles (50 653 amphiphiles) in a cubic box of size $L=49.212\sigma$ at a number density of $\rho=0.85\sigma^{-3}$. Initially, the system is started in the disodered region at the potential depth of $\phi=0.0$ as shown in Fig. 3(a). As we know, a first-order isotropic lamellar transition occurs at the order-disorder transition temperature (T_{ODT}). Then we employ a ''quasistatic cooling'' procedure in which the last configuration at a given ϕ is used as the first configuration at $\phi+\Delta\phi$ with a small increment $\Delta\phi<0.1$ (cf. Fig. 4) to locate the order-disorder transition point in our model system. Figure 4 shows the overall order-parameter S and bulk pressure vs ϕ. At small values of ϕ, order parameter fluctuates around zero; the system is in an isotropic state. With increasing ϕ (''cooling'') the pressure decreases linearly, while S stays roughly constant. At $\phi=1.24$, the transition occurs: S exhibits a sharp jump to $S=0.53$, accompanied by a discontinuous

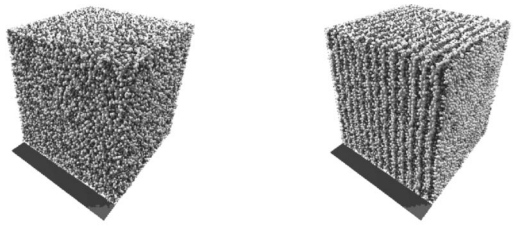

FIG. 3. (a) The isotropic phase at $\phi=0$ and (b) the obtained equilibrium lamellar phase at $\phi=1.3$ for the typical system of $N/2=50\,653$ dimers.

decrease in pressure. By monitoring the configurations, we find that dimers aggregate and first form a multidomain lamellar structure. Then the small lamellar domains merge into a global (on the scale of the box) perfect lamellar phase. This result conforms to theoretical and experimental results that symmetric diblock copolymers, below the critical T_{ODT} only order into lamellae [26,27]. Increasing ϕ further, S increases slightly, turns to level off at a value of about $S=0.62$, while the pressure continues to decrease roughly linear with ϕ. Upon ''quasistatic heating'' we find the reverse order-disorder transition with a pronounced hysteresis. Even slower cooling and heating, as well as the investigation of the smaller systems, does not reduce the hysteresis significantly. Thus we locate the isotropic lamellar phase transition at $\phi_{\mathrm{ODT}}=1.20\pm0.03$. Like in the case of the isotropic smectic transition in liquid crystal systems and finite chain block copolymers, the transition is first order [2]. In addition, the model system even tends to weakly reproduce the chain stretching effect as ϕ increases. For example, as ϕ increases from 0.8 to 1.23, the mean value of the bond length increases from 1.088σ to 1.100σ. For long block copolymers the change in chain extension of course is larger [28].

As shown before [14], the ordered system contains truly 2D liquid layers. To make sure that the starting system is not subject to any anisotropic stress due to the periodic boundary conditions, we first check the pressure tensor in the lamellar phase. The diagonal components of the pressure tensor are equal within the error bars, for example at $\phi=1.3$, we obtain $P_{xx}=P_{yy}=P_{zz}=2.86$. The off-diagonal components are found to vanish. The identification of tensionless lamellar state is needed to compare our findings to experiments and theory. The large difference in the tracer diffusions along the lateral and along the transverse directions further shows that the obtained lamellar system is indeed the fluid lamella. Thus this simple model already gives a rather good physical picture of the equilibrium static lamellar (smectic) state for diblock copolymers, surfactants, and liquid crystals. In the following, We use this lamellar phase at $\phi=1.30$, as shown in Fig. 3(b), to study the shear-induced orientation, unless explicitly mentioned.

After preparing the perfectly ordered lamellar phase, we apply a shear with the shear plane and the shear direction parallel to the layer normal, which is the so-called transverse orientation. For the same initial quiescent configuration, we apply shear rates between $\dot{\gamma}=0.001\tau^{-1}$ and $\dot{\gamma}=0.04\tau^{-1}$, as indicated in Figs. 5 and 6. In this range of shear rates, as it can be derived from the velocity profiles in Fig. 7, the assumption of linearity in the velocity field is valid though not that clearly for the lowest shear rate, as long as we deal with a spacially homogeneous system. Note that the introduced velocity difference between subsequent layers even for the highest shear rate is much smaller than the typical thermal velocity. Table I (a) illustrates the averaged values of the director components n_x, n_y, and n_z, order-parameter S, shear viscosity η, and the strain energy density per time unit $\eta\dot{\gamma}^2$ for the final stationary configurations. Since the equilibrium layer structure is disturbed in the start up of shearing flow, the transverse orientation becomes unstable.

For the very weak shear rate of $\dot{\gamma}=0.001\tau^{-1}$, the transverse lamella first buckle and then become instable. Subsequently, they rotate into a state, where the layers are almost oriented in plane with the shear flow. These tilted lamella

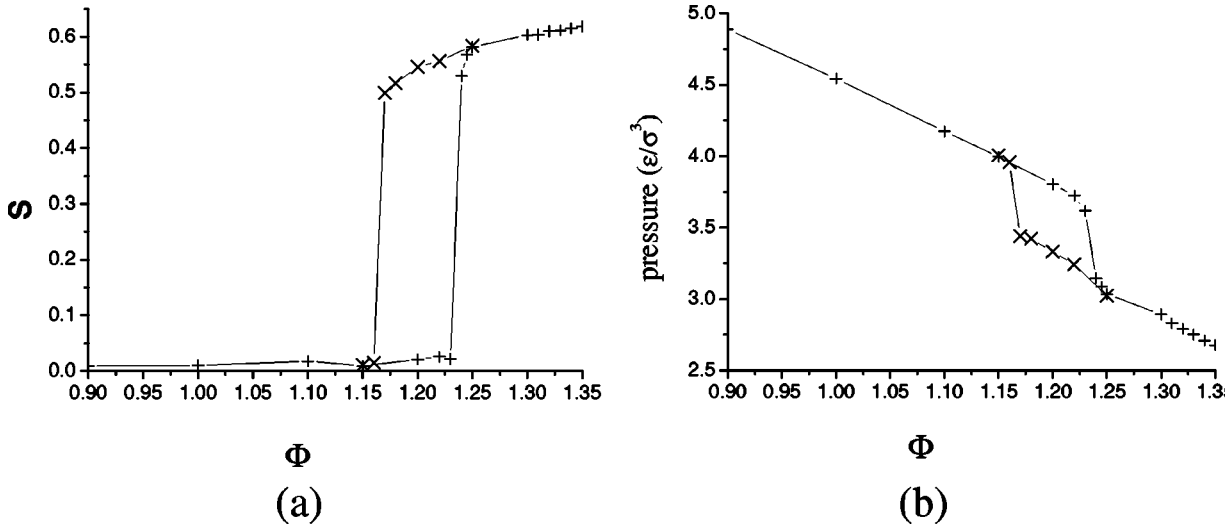

FIG. 4. (a) The averaged order-parameter S and (b) the bulk pressure as a function of the potential depth ϕ. (+) denotes the way from $\phi=0$ to larger ϕ, (×) reverses the direction.

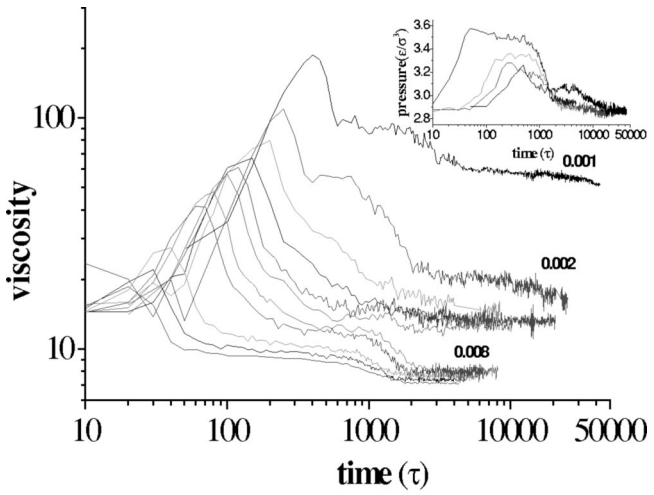

FIG. 5. The variation of shear viscosity in unit of $(m\epsilon/\sigma^4)^{1/2}$ with time for different imposed shear rates. From the top curve to the bottom one, each curve corresponds to the case of shear rate $\dot{\gamma}=0.001$, 0.002, 0.003, 0.004, 0.005, 0.006, 0.008, 0.01, 0.02, 0.03, and $0.04\tau^{-1}$. Inserted, bulk pressure vs time for different shear rates. From the top curve to the bottom one, each curve corresponds to the case of shear rate $\dot{\gamma}=0.03$, 0.004, 0.002, and $0.001\tau^{-1}$.

have a predominant alignment in the parallel orientation of $n_z \approx 0.90$ with non-negligible director components along the other two directions of $n_x \approx 0.31$ and $n_y \approx -0.31$. The order parameter itself settles closely to the value at the starting state. For the shear rates between $\dot{\gamma}=0.002\tau^{-1}$ and $\dot{\gamma}=0.006\tau^{-1}$, the transverse lamella first buckle, then break into a disordered state, finally reorder and evolve into the parallel alignment of $n_z>0.9$. In this regime, with the increase of shear rate, the value of n_y increases slightly, the value of n_z decreases a little, but n_x stays close to zero. From the other studies on this model we know, that eventually we have to expect the perpendicular state as shear rate increases. For the higher shear rate between $\dot{\gamma}=0.008\tau^{-1}$ and $\dot{\gamma}=0.04\tau^{-1}$, similarly the transverse lamella first buckle, then break and dissolve into the disordered state, but later evolve into the perpendicular alignment with $n_y>0.9$. Typical configuration evolutions can be seen in Fig. 7. The detailed analysis of the structural evolution during these orientation transitions will be given in the next two paragraphs. Here we discuss how the macroscopic observables such as instantaneous shear viscosity and bulk pressure change as a shear field with different shear rate is applied. As demonstrated in Fig. 5, first both viscosity and pressure increase rapidly to a transient peak value. This is the characteristic onset of the diverging viscosity and pressure, if one would like to induce creep by shear in an ideal stable solid. The layers are bent, but still resist the flow. This overshoot announces the incidence of the above first stage of alignment transition order $\rightarrow$disorder for $\dot{\gamma}>0.001\tau^{-1}$ and ''order$\rightarrow$less order'' for $\dot{\gamma}=0.001\tau^{-1}$. Then viscosity and pressure drop relatively fast to the typical value for the disordered system, gradually decaying into the typical values of the final stationary state. This gradual decay is indicative of the second stage of the alignment transition disorder$\rightarrow$order for $\dot{\gamma}>0.001\tau^{-1}$ and ''less order$\rightarrow$order'' for $\dot{\gamma}=0.001\tau^{-1}$. For $0.001\tau^{-1}<\dot{\gamma}<0.008\tau^{-1}$, the final phase is aligned parallel, the viscosity varies between $20(m\epsilon/\sigma^4)^{1/2}$ and $12(m\epsilon/\sigma^4)^{1/2}$. On the other hand for $0.008\tau^{-1}\leqslant\dot{\gamma}\leqslant0.04\tau^{-1}$, the final phase is aligned perpendicular, the viscosity varies between $8(m\epsilon/\sigma^4)^{1/2}$ and $7(m\epsilon/\sigma^4)^{1/2}$. The relatively high shear viscosity at $\dot{\gamma}=0.001$ is a consequence of the tilt of the lamella along the unfavorable direction in the shear field. The system is stuck in this situation and we cannot await the final long time relaxation. The shear viscosity is more sensitive to the orientation than the bulk pressure. As expected, the transition from the parallel to the perpendicular alignment accompanies a sharp drop in shear viscosity. A detailed analysis of the complex rheology will be provided in the further publication.

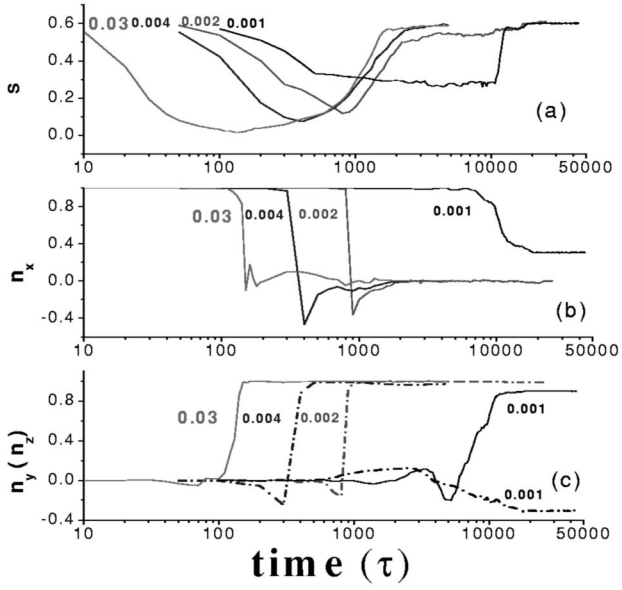

FIG. 6. The temporal evolution of (a) the order-parameter *S*, (b) the component of the director n_x, (c) n_y (black dot-dash and gray solid) and n_z (black solid and gray dot-dash) for the shear rates $\dot{\gamma}=0.001$, 0.002, 0.004, $0.03\tau^{-1}$.

The above analysis via the macroscopic observables pressure and viscosity are supported by the corresponding monitoring of the order parameter and components of director. Figure 6 shows the order-parameter *S* and the components of director n_x, n_y, and n_z vs time for the shear rates $\dot{\gamma}=0.001\tau^{-1}$, $0.002\tau^{-1}$, $0.004\tau^{-1}$, and $0.03\tau^{-1}$. The order-parameter curves show an initial drop and then rise slowly to finally level off. The data for the components of the director more directly mimic the behavior of the viscosity or pressure data. n_x exhibits a steep reduction and levels off close to zero, while n_z or n_y display a significant increase. All these data indicate again that the ordered transverse phase is distorted upon the onset of shear, first buckles or ruptures, and then evolves into an ordered phase oriented in other directions. The only exeption from this is found for the lowest shear rate of $\dot{\gamma}=0.001\tau^{-1}$. n_x does not decay to zero giving the reason for the remaining rather high viscosity. Figure 7 visualizes typical orientation configurations and their velocity profiles at different times. The velocity profile is basically linear in all cases of $\dot{\gamma}\geqslant0.002\tau^{-1}$ despite of some noise.

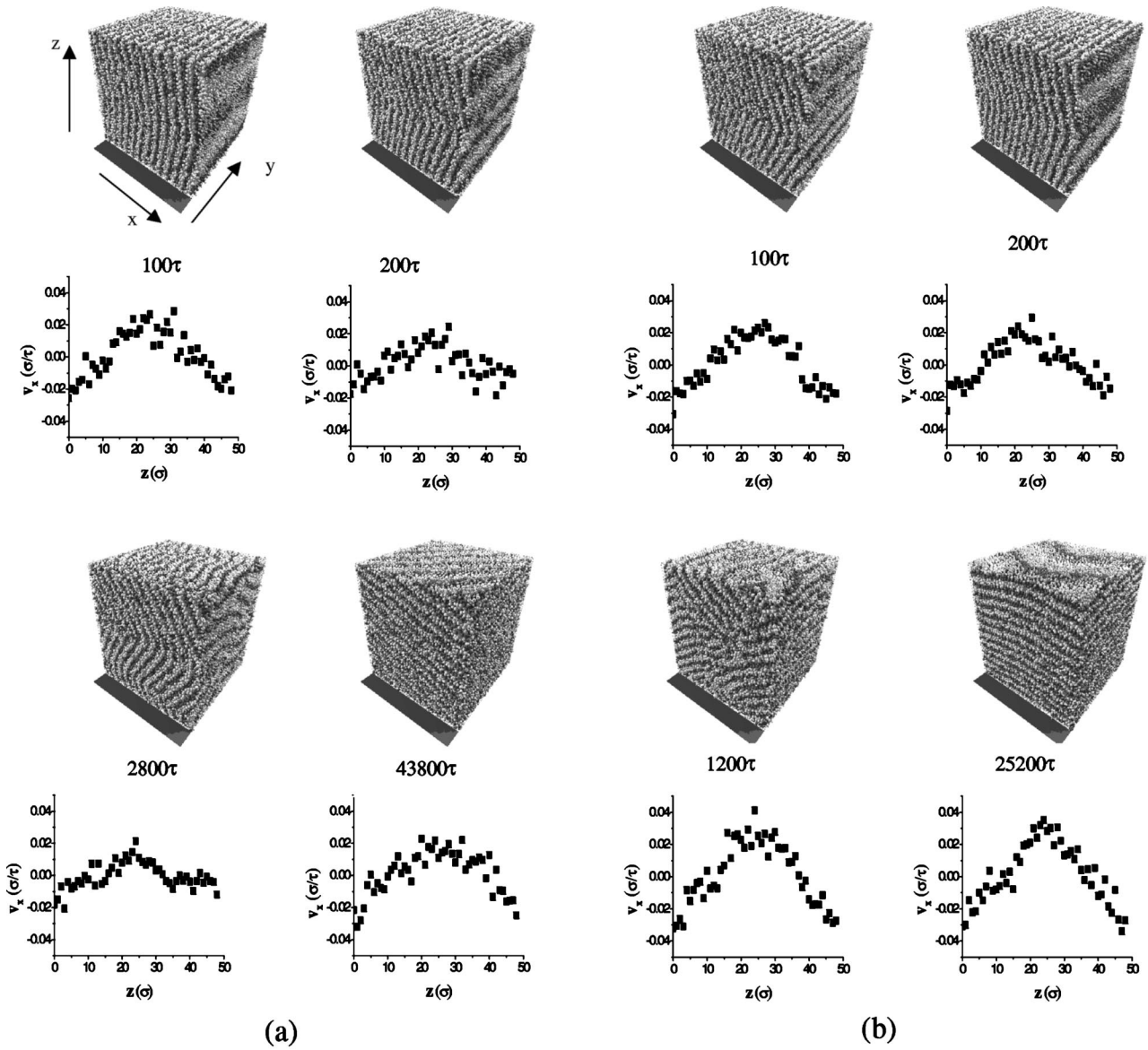

FIG. 7. Simulation snapshots of the time evolution of orientation transition under (a) $\dot{\gamma}=0.001\tau^{-1}$ and their corresponding velocity profile, (b) $\dot{\gamma}=0.002\tau^{-1}$ and their corresponding velocity profile, (c) $\dot{\gamma}=0.004\tau^{-1}$ and (d) $\dot{\gamma}=0.03\tau^{-1}$ and their corresponding velocity profile.

Since the equilibrium layer spacing is disturbed by the onset of the shearing flow, the transverse orientation becomes unstable. As shown in Fig. 7, in order to restore the lamellar spacing to its preferred value, the layers bend along the velocity gradient direction. With the increase of shear rate, the undulation amplitude increases faster. For the very weak shear rate of $\dot{\gamma}=0.001\tau^{-1}$, undulation in Fig. 7(a) tends to rotate the layers into the parallel orientation. The lamellar pattern is not completely torn apart. Both the order parameter and n_x do not decrease to zero. This is related to motion of larger chuncks of pieces of lamella, as is indicated by the nonlinear shear profile [i.e. Fig. 7a, state at 2800τ]. In contrast to that, at higher shear rates, the bending as shown in Figs. 7(b), 7(c) and 7(d) quickly grows large enough to nucleate defects. The layers break and transform to a transient isotropic phase. It can be seen from curves in Figs. 6(a) and 6(b) that the higher the shear rate, the less time it takes for the transverse lamellar phase to melt. For $\dot{\gamma}=0.001\tau^{-1}$, as the value of n_x reduces, both n_y and n_z display distinguished changes, as shown in Fig. 6(c). For $\dot{\gamma}=0.002\tau^{-1}$ and $0.004\tau^{-1}$, only n_z, as plotted in Fig. 6(c), exhibits a strong rise close to one, suggesting that the dimers prefer a parallel alignment in a weak shear flow. Note that this seems to be a direct consequence of the sample history. In a different investigation starting from a multidomain structure, we were not able to stabilize the lamella in the parallel alignment, rather always ended up in the perpendicular state [29]. Beyond this, for $\dot{\gamma}=0.03\tau^{-1}$, only n_y, as drawn in Fig. 6(c), exhibits an abrupt rise to one, indicating that the dimers prefer the perpendicular alignment in a strong shear flow. Note that even at the high shear rate of $\dot{\gamma}=0.03\tau^{-1}$, the instantaneous velocity profile always stays linear.

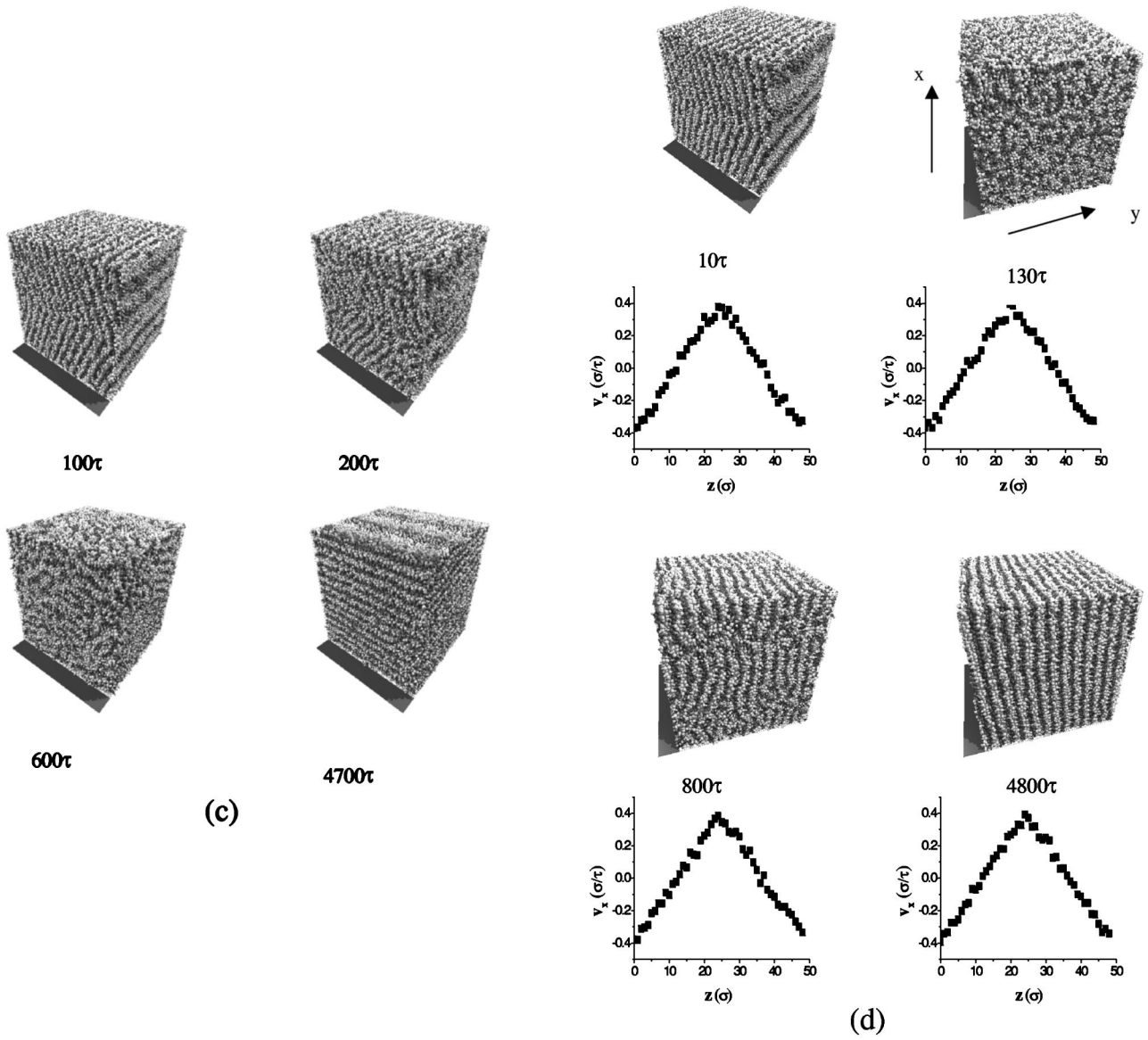

FIG. 7. (*Continued*).

The subsequent transition path is strongly dependent on the shear rate. For low shear rate, the dimers first form short parallel lamellae, then merge into a large lamella in parallel alignment as exhibited in Figs. 7(b) and 7(c). In this case, as shown in Fig. 6, S steadily increases to its peak value about 0.6 and n_z stays near 1.0. In contrary to that, for higher shear rate, dimers first form short perpendicular lamellae, then aggregate into a large lamella in perpendicular alignment as seen in Fig. 7(d). S steadily increases to its peak value 0.59, close to the initial degree of ordering, and n_y remains about 1.0. These results qualitatively conform with experiments and theoretical predictions. For PEP-PEE symmetric block copolymers, for instance, the parallel orientation is found at low shear rate, while the perpendicular one is induced at high shear rate for temperatures near T_{ODT} [9,11]. It indicates again that the simple dimer model properly reproduces the generic dynamic behavior of block copolymer melts or smectic LC systems under shear.

Only the resulting structure for the lowest shear rate in this context poses some questions. Here we obtain the tilted lamella with $S=0.6$, $n_x \approx 0.31$, $n_y \approx -0.31$, and $n_z \approx 0.90$, as displayed in Fig. 7(a). This is the only structure, where the structural evolution always shows a significant degree of order. Thus we should check whether the tilted lamella is resulting from the incompatibility between the box size and lamellar spacing, or represents a metastable phase that should relax towards the pure parallel alignment on sufficiently long time scales. Obviously, as demonstrated by the huge apparent viscosity, the current state is unfavorable. Also this is the only system, though at the smallest shear rate (!), where we find significant deviations from the linear shear profile. By checking the pressure tensor, we find that diagonal components are nearly equal, $P_{xx}=2.874\pm0.024$, $P_{yy}=2.872\pm0.020$, and $P_{zz}=2.897\pm0.031$, and off-diagonal components are vanishingly small. So we can confidently exclude the possibility that the tilt lamellar is constrained by

TABLE I. The shear-rate dependences of the components of the director n_x, n_y, and n_z, and order-parameter S, shear viscosity η in unit of $(m\epsilon/\sigma^4)^{1/2}$, and the strain energy density per time unit $\eta\dot{\gamma}^2$ in unit of $[\epsilon^3/(m\sigma^8)]^{1/2}$ for the stable configurations obtained by shearing the transverse lamella under $\phi=1.3$. (b) The shear viscosity η in unit of $(m\epsilon/\sigma^4)^{1/2}$ and the strain energy density per time unit $\eta\dot{\gamma}^2$ in unit of $[\epsilon^3/(m\sigma^8)]^{1/2}$ for the stable configuration obtained by shearing perfect parallel and perfect perpendicular lamella ($\phi=1.3$) at different shear rates. Averages are taken over at least 3000τ.

(a)

$\dot{\gamma}(\tau^{-1})$	0	0.001	0.002	0.003	0.004	0.005	0.006	0.008	0.01	0.02	0.03
$\langle n_x^2\rangle^{1/2}$	0.999	0.306	0.005	0.002	0.002	0.002	0.002	0.052	0.003	0.015	0.003
$\langle n_y^2\rangle^{1/2}$	0.002	0.306	0.155	0.164	0.231	0.391	0.429	0.994	0.995	0.998	0.997
$\langle n_z^2\rangle^{1/2}$	0.021	0.901	0.987	0.986	0.972	0.920	0.902	0.091	0.099	0.046	0.075
$\langle S\rangle$	0.604	0.601	0.607	0.609	0.595	0.596	0.596	0.585	0.563	0.589	0.587
$\langle\eta\rangle$	∞	51.51	16.34	14.66	13.54	13.23	12.67	8.076	7.938	7.576	7.336
$\eta\dot{\gamma}^2\cdot 10^5$		5.15	6.53	13.19	21.67	33.09	45.62	51.69	79.38	303.05	660.30

(b)

$\dot{\gamma}(\tau^{-1})$	0.001	0.003	0.005	0.007	0.009	0.01	0.013	0.017	0.019	0.02
$\langle\eta\rangle_{para}$	22.13	14.71	13.19	12.84	12.44	12.46	12.41	12.92	12.14	12.08
$\eta_{para}\dot{\gamma}^2\cdot 10^5$	2.21	13.24	32.98	62.95	100.80	124.68	209.88	355.23	438.43	483.48
$\langle\eta\rangle_{perp}$	15.69	9.51	8.56	8.23	7.912	7.88				7.60
$\eta_{perp}\dot{\gamma}^2\cdot 10^5$	1.56	8.56	21.40	40.33	64.08	78.89				304.28

the box size. Prolonging run time e.g., over 5.25×10^6 time step, we found no relaxation process to parallel state. Only by applying a rising shear flow with an incremented step of $\Delta\dot{\gamma}=0.001\tau^{-1}$, n_x gradually decreases but n_z increases. The tilted lamellae transforms into the parallel lamellae at higher shear rate, but the order parameter reduces. Typically our cubic box contains 13 double layers if the lamellae is not tilted against the principal axis of the simulation cell. Counting along the z axis we here find only 12 due to the tilt. This means that shear was too small to completely reorganize the layers. The driving force for local order was larger than the introduced shear stress, eventually also leading to the deviations from a linear strain profile. The reduction of the numbers of sheet leads to an increase in amphiphiles per sheet. This can only fit into the box if the layers are tilted. Any relaxation would require substantial transverse diffusion and (or) or breaking of lamella. For both the shear stress is obviously too small. We expect this to be an artifact of the constant shape of the simulation cell. In an experiment, however, such tilted domains might occur as well. Obviously in our simulation, the orientation transition for the transverse lamella at the very weak shear rate is a transverse→tilt, but at low and high shear rate is an initial fast transverse →isotropic and a later slow isotropic→other preferred orientations, depending on the value of shear rate.

At this point we have to ask, whether for the present system the state parallel to the shear plate can be the preferred one, or would it for larger systems even be preferable to display both, the parallel and perpendicular alignments within the same regime. For this we give in Table I(a) and (b) the shear viscosity and the strain energy density per time unit (energy dissipation rate) for the stable configuration obtained by shearing transverse lamella and by shearing perfect parallel and perfect perpendicular lamella at $\phi=1.3$ and different shear rate. We plot the energy dissipation rate of the final ''steady'' state vs shear rate in Fig. 8. In a nonequilibrium system one expectes the energy dissipation rate to minimize [30]. As one can see from Fig. 8, the data for both the obtained perpendicular and a corresponding perfect perpendicular structure are always somewhat lower than that for the obtained and the corresponding perfectly parallel orientation. Thus the obtained parallel orientations for the present system parameters are a metastable conformations as a result of the competition between the tendency to stick to layered plaquettes and the shear-induced complete reorganization.

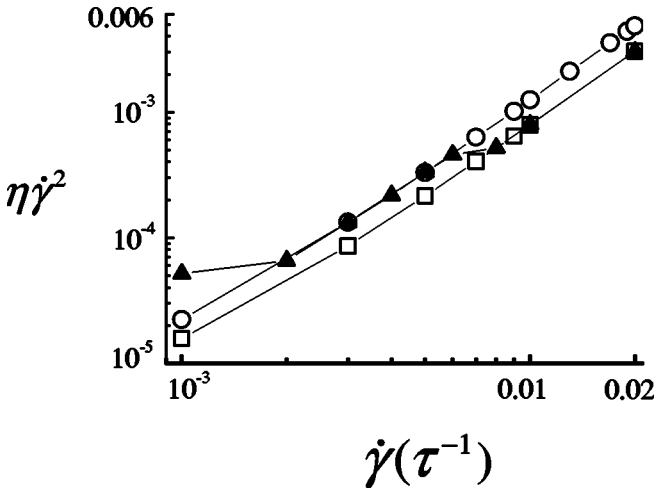

FIG. 8. The strain energy density dissipated per time unit $\eta\dot{\gamma}^2$ in unit of $[\epsilon^3/(m\sigma^8)]^{1/2}$ for the stable configurations obtained by shearing perfect parallel lamellae (open circle) and perfect perpendicular lamellae (open square), as well as for final steady states derived by shearing perfect transverse lamella (filled triangle) under different shear rate.

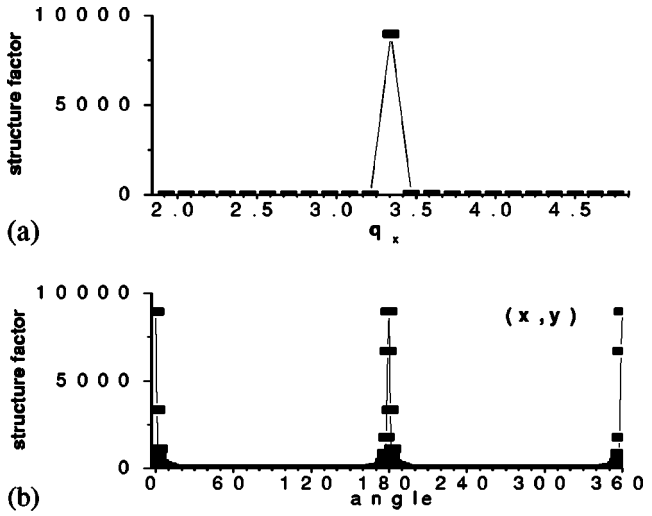

FIG. 9. The structure factor scan for the unperturbed transverse state (a) as a function of the wave vector q along the x direction and (b) as a function of angle at $q=q_0$ in the (x,y) plane.

IV. INTERPRETATION OF EXPERIMENTS

Besides these direct observations of the order, we can also follow the time development of the structure factor, just as it has been done in a recent experiment on shearing transversely ordered smectic liquid crystals [13]. We calculate the time evolution of structure factor

$$S(\mathbf{q})=\frac{1}{N}\sum_{i<j} e^{i\mathbf{q}\cdot\mathbf{r}_{ij}} \tag{11}$$

along the x, y, z, and director axis, as well as in the (x,y), (x,z), and (y,z) planes with $\mathbf{q}$ being commensurable with the box. To clearly display the layer structure, we scatter off the centers of the dimers. Figure 9(a) shows the structure factor $S(\mathbf{q})$ of the initial transverse configuration along the x axis. The single peak at $q_0=3.34\sigma^{-1}$ illustrates the perfect lamellar structure with a well-defined double layer spacing $2\times 2\pi/q_0=3.76\sigma^{-1}$. Then we scan in the (x,y), (x,z), and (y,z) planes for constant $q=q_0(\pm 0.01)$.[1] As expected, the intraplane structure factor, that is in the (y,z) plane, shows no structure at all for this q value. The structure factor in the (x,y) plane and in the (x,z) plane is indistinguishable. As exhibited in Fig. 9(b), three peaks of the same amplitude at 0°, 180°, and 360° in the (x,y) plane indicate the layer normal pointing along the subsequent shear direction. The very same analysis we now perform for the time development of the sheared transverse layers. We apply this to four cases, namely, $\dot{\gamma}=0.001\tau^{-1}$, where the tilted lamella occurred, $\dot{\gamma}=0.002$ and $0.004\tau^{-1}$, where the parallel lamella appeared, and $\dot{\gamma}=0.03\tau^{-1}$ where we find perpendicular lamella. For the tilted lamella as shown in Fig. 7(a), calculating the structure factor along the experimentally accessible planes, no peak appears. This is due to the perfect, but tilted lamella.

[1]Note that $\mathbf{q}$ has to be commensurable with the cubic box, allowing only for discrete values of $\mathbf{q}=2\pi(n_x,n_y,n_z)/L$.

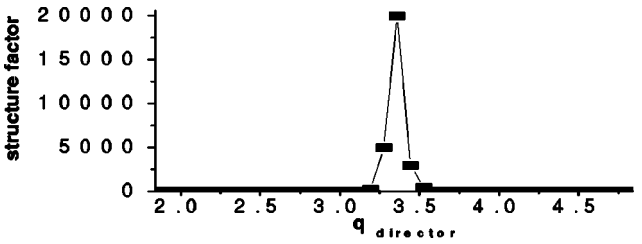

FIG. 10. The structure factor scan for the tilted lamellar state at $\dot{\gamma}=0.001\tau^{-1}$ as a function of q along the director direction.

Only scanning along the director axis, we find a significant peak, as shown in Fig. 10. Furthermore, the maximum value of peak (about 19 922.2) is even larger than that of the starting transverse phase (about 8952.12), demonstrating the shear-induced ordered state, which is obviously subjected to an ordering stress. Actually the director fluctuations are reduced compared to the unsheared state. The time-dependent two-dimensional structure factor scans of the other orientation transitions, e.g., transverse to parallel are shown in Figs. 11(a) and 11(b), and transverse to perpendicular in Fig. 11(c). The transverse lamella first bend and then quickly break. The significant peaks typical of transverse lamella at 0°, 180°, and 360° in (x,y) and (x,z) planes all decrease rapidly. Then structure factor becomes isotropic in any plane. As time elapses, for $\dot{\gamma}=0.002$ and $0.004\tau^{-1}$, the broad peaks around 90° and 270° in the (y,z) plane and (x,z) planes appear, demonstrating the parallel orientation of layers. While for the $\dot{\gamma}=0.03\tau^{-1}$, the broad peaks at 90° and 270° in the (x,y) plane and approximately at 0°, 180°, and 360° in (y,z) planes build up, demonstrating the perpendicular orientation of layers. Subsequent evolution is accompanied by increasing peak heights and sharpening of the peaks. As expected, all these are in good agreement with the above analysis of order parameter, director and snapshots. It is noteworthy that the derived peak height in (x,z) plane for the final stable parallel orientation and the derived peak height in (x,y) plane for the perpendicular orientation are all smaller than the peak values of the starting transverse lamella. By examining order parameter and director component in Table I and snapshots in Fig. 7, it is apparent that the obtained low peak height of the final state in these planes are not due to reduced orientational ordering but from small tilts in the alignment, i.e., $n_x\approx 0.0$ but $n_y\neq 0$ for $\dot{\gamma}=0.002$, $0.004\tau^{-1}$ and $n_x\approx 0.0$ but $n_z\neq 0$ for $\dot{\gamma}=0.03\tau^{-1}$. This is also verified by the scanning results in the (y,z) plane. From the snapshots of Fig. 7, projections of layers in the (y,z) plane are not affected by the tilting. Compared with the peak heights in the corresponding (x,z) or (x,y) plane, the peak heights in (y,z) plane increase dramatically, even larger than the initial transverse peak height for $\dot{\gamma}=0.004$, $0.03\tau^{-1}$. As expected, the more tilted in the (y,z) plane, the lower the peak height is in the corresponding (x,z) or (x,y) plane. In the (y,z) plane, the pure parallel orientation can be manifested by the observation of peak at 90° and 270°. However, since the obtained parallel orientation show a small tilt, peaks emerge at 99° and 279° for $\dot{\gamma}=0.002\tau^{-1}$ and at 104° and 283° for $\dot{\gamma}=0.004\tau^{-1}$. The increase in shift angle with shear rate indicates the tendency to be aligned in perpendicular orientation as shear rate in-

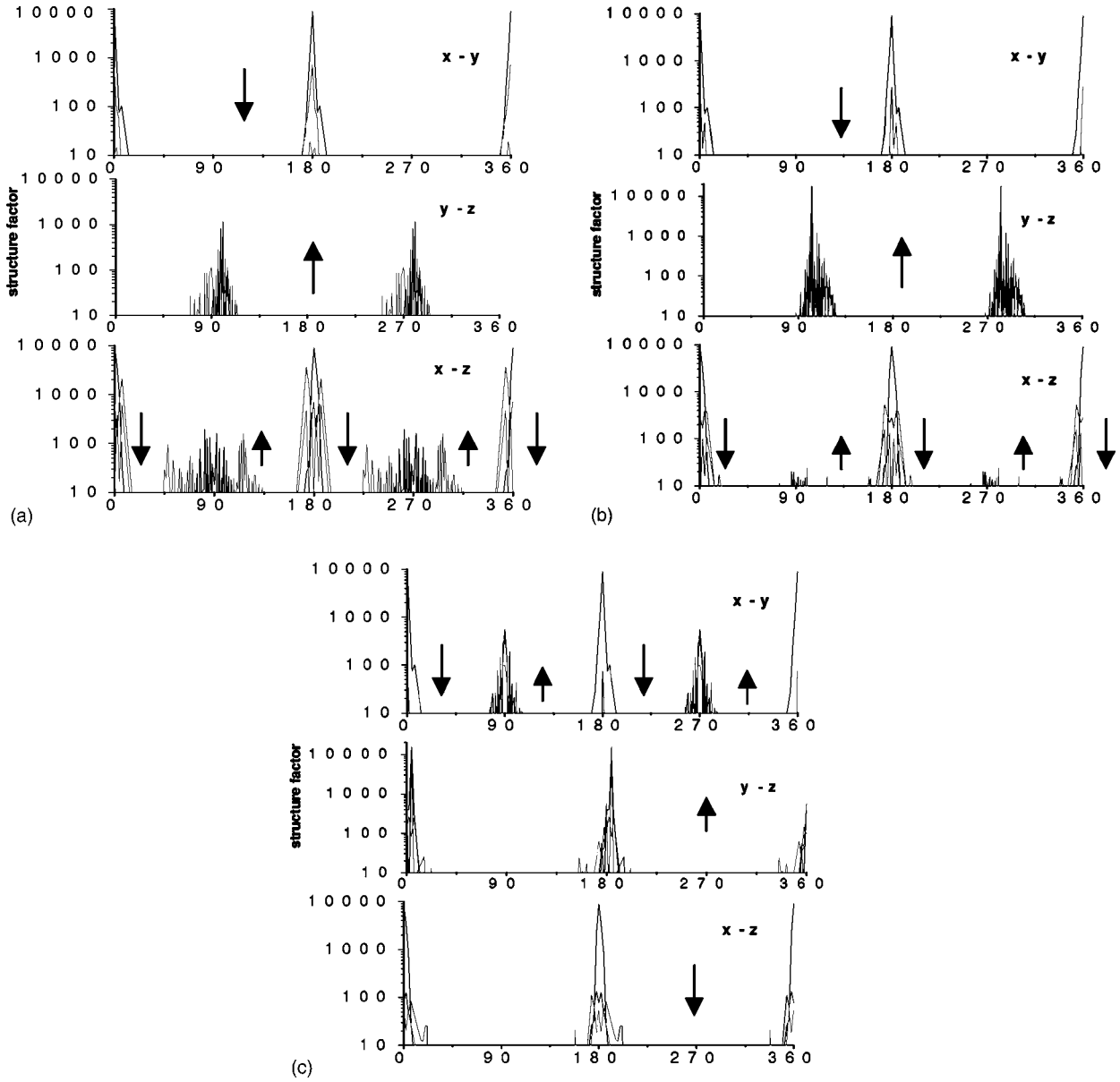

FIG. 11. The evolution of structure factor scan as a function of angle at $q=q_0(\pm 0.01)$ in the (x,y), (y,z), and (x,z) planes at the different shear rate. The arrows indicate the increased shearing time. (a) At $\dot{\gamma}=0.002\tau^{-1}$ for the typical time 0, 50, and 100τ in the (x,y) plane, for the typical time 4500 and 23600τ in the (y,z) plane, and for the typical time 0, 50, and 100 (indicated by down arrows), 4500 and 23600τ (by up arrows) in the (x,z) plane. (b) At $\dot{\gamma}=0.004\tau^{-1}$ for the typical time 0, 50, and 100τ in the (x,y) plane, for the typical time 2000, 2800, and 4700τ in the (y,z) plane, and for the typical time 0, 50, and 100 (by down arrows), 2800, 4700τ (by up arrows) in the (x,z) plane. (c) At $\dot{\gamma}=0.03\tau^{-1}$ for the typical time 0, 10 (by down arrows), 1000, 3000, and 4800τ (by up arrows) in the (x,y) plane, for the typical time 1000, 3000, and 4800τ in the (y,z) plane, and for the typical time 0, 10, and 20τ in the (x,z) plane.

creases. For the perpendicular orientation, the peak position of the maximum is rotated by $\pi/2$ with respect to that of the parallel orientation. The slightly tilted perpendicular orientation of Fig. 7(d) leads to peaks appear at 5° and 185° rather than 0° and 180°, respectively. Besides the tilting of layers, undulations can affect the scattering results. As shown in Fig. 7(b) of parallel lamella at $\dot{\gamma}=0.002\tau^{-1}$, some undulations are present. Undulation in the shear flow direction is studied in detail by Soddeman *et al.* [23,29]. Here we find that this undulation leads to the peak height in the (y,z) plane lower than that of the initial transverse phase. So to identify the alignment and order degree of the shear-induced orientations, it is necessary to scan along several axis and in several planes. Only in this way, we can identify the degree of order and the orientation of the lamellae, and make clear that the difference in the maximum peak of the initial and final phases is due to some weak tilt or due to imperfect ordering with defects in the final state.

V. CONCLUSIONS

The present work shows that it is possible to use large-scale nonequilibrium molecular dynamics simulation with a DPD thermostat to study the shear-induced alignment transi-

tion of diblock copolymer melts, surfactants and liquid crystals in a large-scale system. It is achieved by constructing an effective simplified continuum amphiphilic model. Under shear flow the transverse lamellae first bend. Under very weak shear rate, huge parts of layers gradually rotate to a tilted alignment which has a predominant alignment in the parallel orientation of $n_z \approx 0.90$ and has non-negligible director components along the other two directions of $n_x \approx 0.31$ and $n_y \approx -0.31$. For larger shear rates, the lamellae are torn apart and systems then evolve from the isotropic state into the ordered lamellar state which has a parallel orientation at low shear rate and a perpendicular alignment at high shear rate, basically in agreement with experiments and theory. From measuring the energy dissipation rate, we find that the perpendicular alignment for the present system is more favorable. However, the obtained parallel conformations turn out to be metastable for the present system. Mapping this onto experiment, we expect for typical small layer forming molecules (mesogenes forming smectics or small amphiphiles like lipids) due to the small intralayer friction a strong tendency of a transition into the perpendicular state. The predicted parallel alignment in the limit of the very weak segregation regime [31] will be very difficult to detect, as this regime almost does not exist for the present systems. However, by varying the in plane friction (e.g., variable chain length) the two curves describing the energy dissipation rate in the parallel and perpendicular state of Fig. 8, can be shifted against each other, which eventually also leads to a situation where the parallel orientation is the preferred steady state. To identify the alignment and order degree of the shear-induced orientation by scattering spectra, it is necessary to scan along several axis and in several planes. From our experience, the low peak of the final perpendicular alignment in the spectra of Fig. 3(c) in Ref. [13] may originate from either of the following effects: (i) the final perpendicular phase is less ordered with defects or (ii) it is in a slightly tilted perpendicular alignment. In the future, we will use the same method and vary the monomer properties of the model to investigate the nonequilibrium dynamical behavior pertinent to the diblock copolymer melts, surfactants, and liquid crystals. This might shed light in unveiling the underlying mechanisms for shear effect on the anisotropic complex fluids having different morphologies.

ACKNOWLEDGMENTS

We thank B. Dünweg, H. Pleiner, and J. Vollmer for helpful discussion and critical comments on the manuscript (J.V.).

[1] L. Leibler, Macromolecules **13**, 1602 (1980).
[2] G. H. Fredrickson and E. Helfand, J. Chem. Phys. **87**, 697 (1987).
[3] F. S. Bates and G. H. Fredrickson, Annu. Rev. Phys. Chem. **41**, 525 (1990).
[4] K. I. Winey, E. L. Thomas, and L. J. Fetters, Macromolecules **25**, 2645 (1992).
[5] D. A. Hadjuk *et al.*, Macromolecules **27**, 4063 (1994).
[6] R. G. Larson *et al.*, Rheol. Acta **32**, 245 (1993).
[7] V. K. Gupta, R. Krishnamoorti, and J. A. Kornfield, Macromolecules **28**, 4464 (1995).
[8] O. Diat, D. Roux, and F. Nallet, J. Phys. II **3**, 1427 (1993); J. Phys. IV **3**, 193 (1993); Phys. Rev. E **51**, 3296 (1995).
[9] K. A. Koppi *et al.*, J. Phys. II **2**, 1941 (1992).
[10] C. R. Safinya *et al.*, Science **261**, 588 (1993).
[11] G. H. Fredrickson, J. Rheol. **38**, 1045 (1994).
[12] F. Drolet, P. Chen, and J. Viñals, Macromolecules **32**, 8603 (1999).
[13] Y. Golan, A. M. Herranz, Y. Li, C. R. Safinya, and J. Isaelachvili, Phys. Rev. Lett. **86**, 1263 (2001).
[14] T. Soddemann, B. Dünweg, and K. Kremer, Eur. Phys. J. E **6**, 409 (2001).
[15] G. R. Luckhurst and G. Saielli, J. Chem. Phys. **112**, 4342 (2000); M. A. Bates and G. R. Luckhurst, *ibid.* **110**, 7087 (1999).
[16] R. Goetz and R. Lipowsky, J. Chem. Phys. **108**, 7397 (1998); R. G. Larson, *ibid.* **91**, 2479 (1989).
[17] K. Binder, Adv. Polym. Sci. **112**, 118 (1994).
[18] R. G. Larson, Macromolecules **27**, 4198 (1994).
[19] G. S. Grest and K. Kremer, Phys. Rev. A **33**, 3628 (1986).
[20] K. Kremer and G. S. Grest, J. Chem. Phys. **92**, 5057 (1990).
[21] D. Morse and S. Milner, Phys. Rev. E **47**, 1119 (1993).
[22] F. Müller-Plathe, Phys. Rev. E **59**, 4894 (1999); P. Bordat and F. Müller-Plathe, J. Chem. Phys. **116**, 3362 (2002).
[23] T. Soddemann, G. K. Auernhammer, H. X. Guo, B. Duenweg, and K. Kremer (unpublished).
[24] P. G. de Gennes and J. Prost, *The Physics of Liquid Crystals* (Clarendon, Oxford, 1993).
[25] M. P. Allen and J. Tildesley, *Computer Simulation of Liquids* (Clarendon, Oxford, 1987).
[26] M. W. Matsen and F. S. Bates, Macromolecules **29**, 1091 (1996).
[27] J. D. Vavasour and M. D. Whitemore, Macromolecules **26**, 7070 (1993).
[28] K. Almdal, J. H. Rosedale, and F. S. Bates, Phys. Rev. Lett. **65**, 1112 (1990).
[29] T. Soddemann, Ph.D thesis, Johannes Gutenberg-Universität, Mainz, Germany, 2001. Available at http://www.mpip-mainz.mpg.de/theory.html
[30] D. J. Evans and G. P. Morris, *Statistical Mechanics of Non-Equilibrium Liquids* (Academic Press, London, 1990).
[31] A. N. Morozov, Ph.D thesis, University Groningen, The Netherlands, 2002.
[32] S. S. Sarman, D. J. and P. T. Cummings, Phys. Rep. **305**, 1 (1998).